IASMiRT

SMiRT 26
50 Anniversary Berlin/Potsdam

Transactions, SMiRT-26
Berlin/Potsdam, Germany, July 10-15, 2022
Division VII

CREEP RUPTURE ANALYSIS OF THE RCS PRESSURE BOUNDARY FOR A PWR SBO ACCIDENT

Kwang-Il Ahn[1], Keo-hyoung Lee[2]

[1] Principal researcher, KAERI, Daejeon, Rep. of Korea (kiahn@kaeri.re.kr)
[2] Director, FNC Technology Co., Ltd., Yongin-si, Gyeonggi-do, Rep. of Korea

ABSTRACT

The thermally-induced creep rupture, which could take place on the reactor coolant system (RCS) pressure boundary during a high-pressure accident like a station blackout (SBO), is one of the factors that can affect the ensuing accident behaviours. This paper presents best-estimate analysis results for a possibility of the creep rupture for the RCS pressure boundary for the SBO accident of a reference pressurized water reactor (PWR, APR1400). For the purpose, dedicated modelling was performed for a broad spectrum of plant systems and relevant phenomena influencing the creep rupture: (a) a computational fluid dynamics (CFD) analysis to determine the physical parameters associated with the natural circulation, and then (b) a coupled analysis of MELCOR and CFD to predict the integral responses of the reactor and RCS loop to a severe accident initiated by the SBO sequences. The influence of particular MELCOR modelling schemes and plant conditions in estimating RCS creep rupture characteristics was investigated through relevant sensitivity analyses. The results of the analysis and relevant insights were summarized in terms of particular points of interest and remaining uncertainty issues for further study.

1. INTRODUCTION

In nuclear power plants (NPPs), one of the important but uncertain phenomena during high pressure accidents like a station blackout (SBO) is the possibility for a counter-current natural circulation flow between the hot legs (HLs) and the steam generators (SGs), which could divert the core melt progression and/or the in-vessel fission product (FP) distribution. This, in turn, could lead to a heat-up and eventually creep rupture of the reactor coolant system (RCS) pressure boundary (including the HL nozzles and piping, pressurizer surge line, and SG tubes). From the risk and accident management points of view, key concerns are not only to predict more explicitly whether such a creep rupture can occur in the RCS pressure boundary, but also when and where it is most likely [USNRC, 1998, 2012; Bang et al. 2012]. For example, if a thermally-induced failure sufficient to depressurize the RCS primary side develops in another RCS location prior to the SG tube failure, the possibility for thermally induced-steam generator tube rupture (TI-SGTR) will be significantly decreased. Alternatively, if another RCS component fails shortly after SG tube failure, the rate of mass flow from the primary system to the secondary system could be significantly reduced, and thus the ensuing FP release into the environment through the failed SG tubes and safety valves such as the main steam safety valve (MSSV) could be minimized. Plant-specific RCS and SG design and configuration could also highly influence the pattern of the natural circulation and relevant thermally-induced creep rupture of the RCS pressure boundary [INEL, 1996; USNRC, 2016].

The primary objective of this paper is to present the potential characteristics of a natural circulation-induced creep rupture of the RCS pressure boundary, as implemented as part of the APR1400 SOARCA (State of the Art Reactor Consequence Analysis) study [Ahn & Hwang, 2017; KHNP, 2019]. Two types of SBO sequences were considered for this purpose: long-term and short-term SBO (LTSBO and STSBO, respectively). While the LTSBO sequence assumes that the turbine-driven auxiliary feedwater pump (TD-

AFWP) is available, the STSBO sequence assumes that it is unavailable, consequently leading to a more severe plant condition compared to LTSBO. CFD (Computational Fluid Dynamics) analysis was performed to precisely determine the relevant physical parameters characterizing the behaviour of natural circulation and the ensuing RCS creep rupture. MELCOR2.2 [SNL, 2017] was used to predict the integral responses of the reactor and RCS loop to a severe accident initiated by the SBO sequences. The influence of particular MELCOR modelling schemes and plant conditions in estimating RCS creep rupture characteristics was investigated through relevant sensitivity analyses.

2. MODELING AND ASSUMPTIONS

2.1. Design features of the APR1400

The reference PWR (pressurized water reactor), the APR1400 (Advanced Power Reactor 1400 MWe) [Kim, 2017], is a generation III reactor of two primary coolant loops, with each loop having one SG and two reactor coolant pumps (RCPs) attached in one HL and two cold legs (CLs) arrangement. The pressurizer is connected to one of the HLs to maintain a nominal operating pressure and temperature of the RCS. Shin Kori units 3 & 4 [KHNP, 2011] are the first generation of plants employing the APR1400 design.

2.2. Modeling of RCS loop, core, and RPV

Fig. 1 illustrates the hydrodynamic nodalization scheme of the RCS loop 2 to simulate the natural circulation between the RPV and the SG. For reference, the present MELCOR model defines the RCS loop connected to the pressurizer as the loop 1; otherwise loop 2. The HL was split into two hydrodynamic control volumes (CVs) in the direction of flow, namely upper (CV411/CV413) and lower (CV412/CV414) sides, with each side having its own flow direction. The hydrodynamic flow paths (FLs) connecting the HL upper side with the lower side (FL421/FL422) were modeled to be blocked when a counter-current natural circulation develops inside the HL.

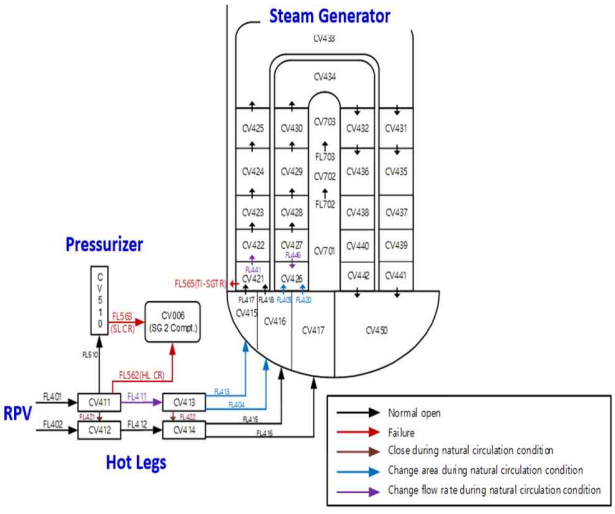

Figure 1. Nodalization of the HL & SG.

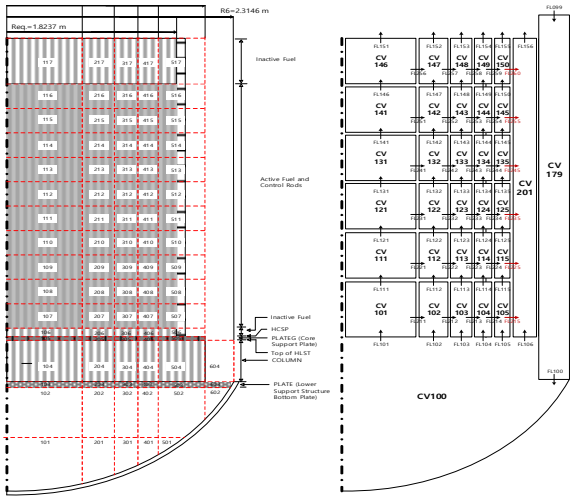

Figure 2. Nodalization of the core and RPV.

The pressurizer connected with the HL through the surge line (CV510) was modeled as a single node (CV500). Since the pressurizer surge line of the APR1400 is mounted on the HL upper side (top-mounted), only the hot fluid of the HL upper side can enter into it. For this reason, the FL from the HL into the surge line was modeled as a single path. Each steam generator includes explicit modeling of U-tubes,

inlet and outlet plenums, and SG secondary side. The SG inlet plenum was subdivided into three regions: a hot region (CV415), a mixing region (CV416), and a cold region (CV417). The SG U-tubes were subdivided into three regions: an up-flowing zone (CV421–CV430), a parallel zone (CV433/CV434), and a down-flowing zone (CV431–CV442).

Fig. 2 also shows the detailed hydrodynamic nodalization model of the RPV and corresponding spatial divisions of the reactor core. The reactor core is represented by five concentric radial rings, with each ring divided into six vertically-stacked hydrodynamic CV nodes. In the core region, axial and radial FLs were defined to simulate two-dimensional flow patterns of the fluid, with each FL simulating the effect of flow blockage and a change in the flow resistance during core degradation.

The RPV lower head (LH) (CV100) was divided into six radial sub-nodes with five axial segments. Ring 6, which is not included in the active fuel region, simulates the outer radial region beneath the vessel downcomer (CV179). The top node of the five axial cells in the RPV LH simulates the core support plate, allowing for a partial collapse by each radial ring. Similar to the reactor core, the upper plenum was divided into five radial rings, with each ring having corresponding axial nodes. To simulate a thermal behavior through it in more detail, the RPV LH wall was divided into 10 segments in a radial direction.

2.3. Models used for the present analysis

2.3.1. FP initial inventory/decay heat

The initial inventories of the FPs and resultant decay heat could influence the temperature of the fluids inside the RCS pressure boundary and the thermal behaviour of the RCS piping network. These are mostly affected by the average effective irradiation time for the entire core. Thus, for the three fuel cycle stages (EOC: end of cycle, MOC: middle of cycle, and BOC: beginning of cycle), the corresponding fuel burnups were derived taking into account the average burnup per cycle, average fuel cycle, power distribution in the equilibrium core, and irradiation time period for the entire core. An average fuel burnup of 17571 MWD/MTU (based on 458 operating days) was used in the present analysis.

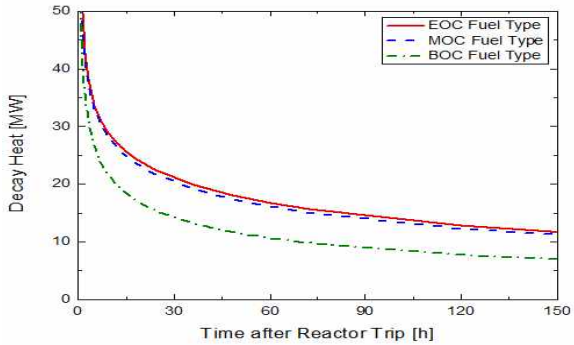

Figure 3. Decay heat curves for three fuel cycle stages.

The ORIGEN (Oak Ridge Isotope GENeration) code [Ryman, 2000] was employed to estimate the corresponding initial inventories and the decay heat with time was evaluated using the ANS decay model [ANS, 2014]. Fig. 3 shows characteristic decay heat curves for the three fuel cycle stages

2.3.2. Decay heat of FPs inside the RCS

As the accident progresses, FPs are deposited on the RCS heat structures, and the resultant decay heat could either be absorbed into the fluid and the pipe walls or transferred to the outside of the pipes. The MELCOR default value assumes that half of the FP decay heat is absorbed by the fluid and vapour inside the HL pipe

and the other half is absorbed into the steel pipe walls. Whereas, the US SOARCA study [USNRC, 2012, 2013] assumes the decay heat to be distributed over the primary system and piping as follows: 25% and 74.38% of the decay heat from the FPs inside the HL piping are allocated into the vapour inside the piping and to the pipe walls, respectively, with the remaining 0.62% transferred to the outside of the piping. The present study employed the foregoing approach.

2.3.3. CFD analysis of natural circulation flows

A best-practice experience from the US SOARCA study indicates that the counter-current natural circulation flow between the HL and the SG would develop with a high potential when the HL void fraction exceeds 0.95 and the degree of superheat in the HL exceeds 10 K. If either the RCS loop seal is cleared or the RCS boundary is open due to the failure of the HL or a stuck-open of POSRV, the natural circulation flow will cease. However, plant-specific design characteristics of the RCS and the SG could strongly influence the pattern and behaviour of natural circulation [USNRC, 2010, 2016].

From the phenomenological point of view, the natural circulation flows between the RPV upper plenum and the SG are mainly controlled by the flowrate, density, and temperature of the fluid [USNRC, 2010]. These parameters are directly related to the following five dimensionless parameters: (a) discharge coefficient, (b) recirculation ratio, (c) mixing fraction, (d) fraction of the hot SG tubes, and (e) normalized temperature of the hottest SG tubes. Whereas, MELCOR does not implicitly model the mixing of fluids in the RCS loop, but instead employs relevant predetermined mixing and flow parameters. Accordingly, a CFD analysis [ReTECH, 2019], which is based on FLUENT Version 6.3, was carried out to determine more precisely the foregoing physical and dimensionless parameters, based on the RCS/SG configuration in Fig. 1. For reference, the present modelling assumptions are consistent with the previous works [USNRC, 2004, 2010, 2016] in terms of settings of numerical solver, turbulence options, and density of the general nodes. Fig. 4 and Table 1 summarize the CFD analysis results, estimated based on the foregoing process.

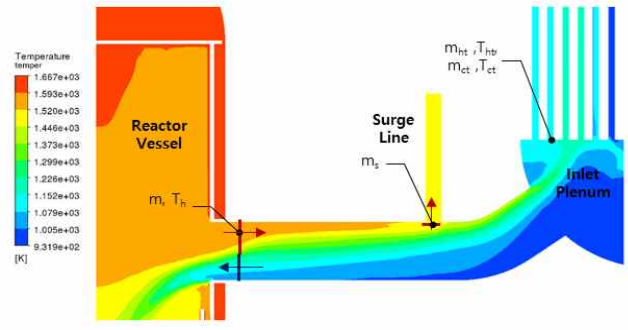

Figure 4. Fluid temperature profile.

Table 1: Physical parameters driving the natural circulation.

Parameters	Values
C_D (discharge coefficient)	0.11
r (recirculation ratio)	3.5
f (mixing fraction)	1.0
F (hottest tube fraction)	0.49
T_n (normalized temperature of hottest tubes)	0.44

2.3.4. MELCOR application of the CFD results

Based on the CFD analysis results, a discharge coefficient of 0.11 and a recirculation ratio of 3.5 were applied to the MELCOR model to comply with the natural circulation flow through the HL and the recirculation flow through the SG, respectively. A mixing fraction of 1.0 means that the fluid is well mixed in the SG inlet plenum to a single temperature distribution. Thus, the three nodes of the SG inlet plenum for the MELCOR analysis (CV415, CV416, and CV417) were merged into a single node, and the user-controlled pump functions applied to adjust the areas of the corresponding flow paths (FL404, FL405, FL413, and FL420) were removed as well. The estimated SG hot tube fraction of 0.49 implies that almost half of both hot side and cold sides of the SG tubes were partitioned into the same area. The estimated

normalized hottest tube temperature of 0.44 was conservatively applied to the tube piping temperature with the assumption that the hottest temperatures of the fluid and the wall of the SG tubes are the same.

While the HL nozzle and piping was modeled as a single fluid node subject to the same temperature, the fluid between the RPV outlet nozzle and the SG inlet nozzle has a temperature gradient during the natural circulation. As a result, the HL nozzle could be higher than that of the HL piping. Referring to the US SOARCA approach [USNRC, 2012, 2013], the heat transfer coefficient of the RPV outlet nozzle conservatively increased 1.5 times. Flow blockage models in the core were utilized to simulate the natural circulation flow during core degradation.

2.3.5. Creep rupture of the RCS pressure boundary

The piping stress analytical module (PIPE-STR) and the Larson-Miller lifetime damage model (LM-CREEP) built into the MELCOR code were utilized to estimate the creep rupture damage indices of the RCS pressure boundary. The creep rupture model was applied to the following components of the RCS boundary: (a) the HL nozzle and piping (carbon steel), (b) pressurizer surge line (stainless steel), and (c) SG U-tubes [Alloy (Inconel) 690]. The Larson-Miller (LM) parameter and the time required for the creep failure of the HL piping, nozzle and pressurizer surge line were calculated using the default values in MELCOR. The LM parameter and cumulative time to creep failure of the SG U-tubes were calculated utilizing the creep rupture model employed in MELCOR. For reference, the LM creep rupture model assumes that a creep rupture of each component takes place when the corresponding creep rupture damage index reaches 1.0.

2.3.6. Failure of the RPV LH

The MELCOR code employs dedicated mechanisms and relevant models for the RPV LH failure as follows:

- LH penetration tube failure: parametric model, assuming a failure of the welding material at whose melting point 1273.15 K;
- LH wall creep rupture: Larson-Miller (LM) parametric model or 1-D mechanical model.

The Surry SOARCA [USNRC, 2013] recommends a LH creep rupture as the most probable failure mechanism. To reflect such a trend, the present analysis employed the same approach as the Surry SOARCA project, assuming an initial break size of 0.1 m diameter. As the RPV LH and penetration tube materials, the APR1400 adopts stainless steel-coated carbon steel and stainless steel, respectively.

2.3.7. Stuck-open of POSRV and MSSV

During a high-pressure nuclear accident like SBO, the POSRV could be stuck-open due to its cyclic operation according to the pressure posed on it, from which the possibility for counter-current natural circulation flows between the RPV upper plenum and SG increases followed by a potential creep rupture at any location of the RCS loop.

In the APR1400, four POSRVs and ten MSSVs are placed on the pressurizer and the main steam line, respectively. The blowdown pressure of each valve was designed to be 13% for the POSRV and 8% for the MSSV, greatly reducing the possibility of these valves becoming stuck open. Relating to their stuck-open failure expected during the accident progression, however, there is no currently available relevant data in the case of the APR1400, e.g., when it happens and under what conditions. Thus, the present analysis assumes that MSSV stuck-open happens when the cyclic operation of the first MSSV exceeds a pre-defined frequency (number).

2.4. Modeling of the SBO sequences

The present LTSBO scenario is a core damage sequence induced by a complete loss of all onsite and offsite alternating current (AC) powers. All safety systems being driven by AC power are unavailable, but a direct current (DC) battery lasting for 8 h is available to run the TD-AFWP of 100% capacity and POSRV three-way valves. According to the APR1400 PSA [KHNP, 2011], this accident sequence leads to a core damage frequency (CDF) of 6.36E-07/ry, taking up 57.3 % of the internal initiating events CDF. The STSBO scenario, which is induced by a seismic event in the case of the APR1400, is almost the same except that the TD-AFWP is unavailable in this scenario. As a result, the accident progresses to core damage much faster compared to the LTSBO sequence. This accident sequence leads to a CDF of 3.43E-07/ry. For the accident analysis, additional conditions in Table 2 [KHNP, 2017] were assumed for the base scenario.

Table 2: Additional plant conditions assumed for the base scenario.

	LTSBO	STSBO
RCP seal leakage	Not considered	
TD-AFWP	Actuated using the mobile emergency diesel generator (EDG) just before the DC battery is depleted to make up the SG secondary side	N/A
POSRV three-way valves	Aligned at around 10 min before the DC battery is depleted, to divert the effluent containing hydrogen from the primary system to the SG compartment during a severe accident.	Aligned at around 10 min after reaching the severe accident management (SAMG) entry condition [when the core exit temperature (CET) exceeds 649 ℃ (922.15 K)]

3. RESULTS AND FINDINGS

3.1. Base case analysis

Table 3 summarizes the timings of the key events in the two base scenarios predicted by the MELCOR code until 24 h after the accident. The subsequent sections describe the analysis results of interest in more detail.

Table 3: Timings of key events in the two SBO sequences (base case).

Key Events	LTSBO (h)	STSBO (h)
SBO (Reactor and RCP trip)	0.0	0.0
MSIVs (main steam isolation valves) close	0.001	0.001
TD-AFWP start	0.02	–
MSSVs open	0.05	0.04
SG 2 dryout	2.0	1.7
TD-AFWP stop	8.0	–
SG 1 dryout	10.3	1.6
Pressurizer POSRVs open	10.6	1.9
Core (top of active fuel) uncover	11.9	2.8
CET exceeding 649 ℃ (922.15 K)	12.9	3.4
Creep rupture of HL nozzle in the RCS loop 2	15.1	–
Relocation of core debris onto the RPV LH	19.1	5.5
Failure of the RPV LH	19.7	5.8

3.1.1. LTSBO scenario

Fig. 5(a) shows that the fluid temperature in the HL was the highest compared with other RCS pressure boundaries, owing to its close proximity to the hot gases exiting the RPV. As a result, the HL nozzle was first predicted to fail by creep rupture at 15.1 h, as identified in Fig. 5(b). As the RCS pressure decreases after the HL ruptured, the SIT started to inject a cooling water and for a while, recovered the water level of the primary system. After the SIT inventory dries out, the water level of the primary system rapidly decreased again and the RPV LH failed at 19.7 h (see Table 3). No failure of the SG U-tubes was predicted by the end of the calculation time.

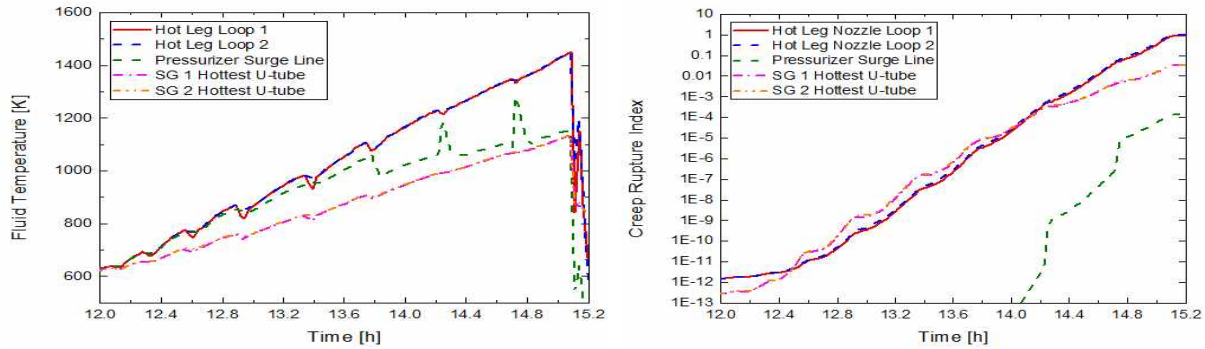

(a) Natural circulation flow fluid temperature (b) Creep rupture damage index

Figure 5. LTSBO analysis results (base case).

3.1.2. STSBO scenario

According to Fig. 6(a), the fluid temperature increased as the natural circulation flow started to develop, but as the pressurizer water level increased, the fluid temperature began to decrease after 4.8 h. Until the pressurizer dried out and the surge line is cleared (just before 4.8 h), the vaporized fluid inside the pressurizer was released into the containment through the opened POSRV, consequently decreasing the fluid temperature. As a result, the rate of the creep rupture damage indices slowly increased with time and the RCS pressure boundary maintained its integrity, as shown in Fig. 6(b). In contrast, the RPV LH failed at 5.8 h (see Table 3), and thereafter additional creep rupture did not occur in the RCS pressure boundary.

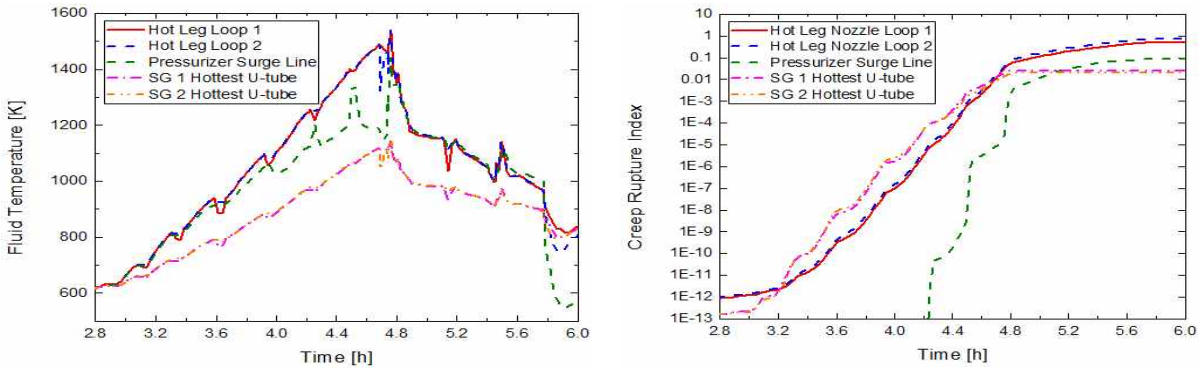

(a) Natural circulation flow fluid temperature (b) Creep rupture damage index

Figure 6. STSBO analysis results (base case).

3.2. Sensitivity analyses

3.2.1. LTSBO scenario

A couple of sensitivity analyses were carried out for two plant conditions that might influence the thermal behavior of the RCS pressure boundary: (a) a stress multiplier on the SG U-tubes and (b) a stuck-open failure of the MSSV.

(1) Case 1: Influence of SG U-tube stress multiplier

According to the US SOARCA study, TI-SGTR took place first prior to a failure of the HL pipe and pressurizer surge line in the case that SG tube vulnerability was augmented with a stress multiplier of 1.5. The same assumption was applied to the present analysis, and Fig. 7(a) shows the resultant creep rupture index of each RCS pressure boundary. Compared to the corresponding base case analysis results, the creep rupture damage indices of both SG U-tubes increased by about 6 times. Nevertheless, the HL nozzle again failed first, prior to SG U-tube failure.

(2) Case 2: Influence of stuck-open MSSV

During the high-pressure severe accident progression, the MSSV continually repeats opens and closes due to the heat transferred from the RCS, and eventually it may become stuck open due to the high temperature fluid passing through the valve. When MSSVs are stuck open, the SG can be depressurized up to atmospheric pressure. As a result, the differential pressure between the primary and secondary sides of the SG increases the material stress of the SG U-tubes. Taking into account this situation, a sensitivity analysis was carried out to find the influence of MSSV stuck-open failure. The corresponding sensitivity analysis shows that the MSSV became stuck-opened at 13.6 h, which caused SG 1 to depressurize to atmospheric pressure. After that, the creep rupture index of the SG 1 tubes increased sharply, as shown in Fig. 7(b), with a rupture eventually occurring at 14.8 h. Nevertheless, the creep rupture damage index of the HL nozzle also continuously increased, eventually failing at 15.2 h. This result indicates that TI-SGTR will not preclude the ensuing HL creep rupture, and also that the RCS creep rupture could happen in other locations even after TI-SGTR.

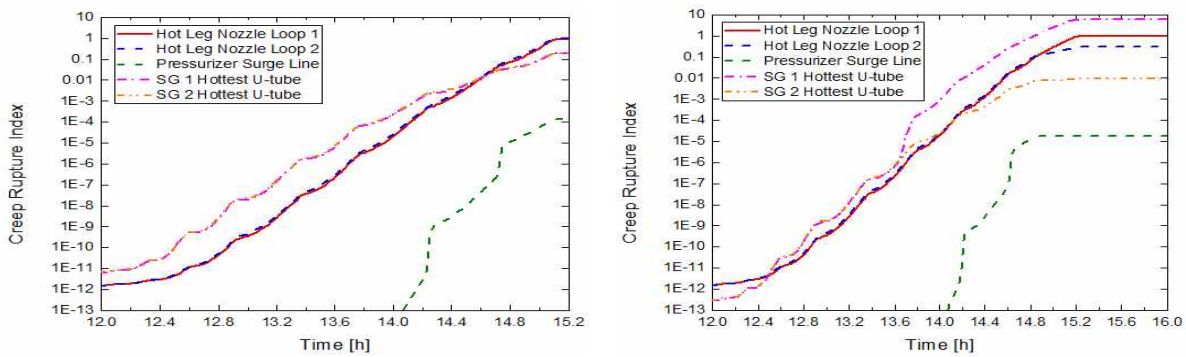

(a) Creep rupture damage index (case 1)

(b) Creep rupture damage index (case 2)

Figure 7. LTSBO analysis results (sensitivity cases).

3.2.2. STSBO scenario

Fission product decay heat could influence on the pattern of natural circulation in the RCS pressure boundary and relevant creep rupture characteristics. For example, the decay heat was removed in the LTSBO sequence as the TD-AFWP supplied feedwater to the SG, consequently leading to a creep rupture of the HL prior to the dryout of the pressurizer. In contrast, decay heat was not removed in the STSBO sequence, consequently leading to a dryout of the pressurizer and a decrease of the natural circulation fluid

temperature prior to creep rupture. Taking into account this situation, a couple of sensitivity analyses were carried out with the respective decay heat curves estimated for MOC and BOC in Fig. 3.

(1) Case 1: Influence of the BOC fuel type

For the BOC fuel type, the natural circulation flow developed over 3.6 h to 6.8 h, as shown in Fig. 8(a). While the RPV LH failed first in the base case, results for the BOC fuel showed that the pressurizer did not dry out during the natural circulation and the RCS fluid temperature kept increasing until the natural circulation terminated. Consequently, the creep rupture index of the HL nozzle connected to the pressurizer surge line exceeded 1.0 at 6.7 h.

(2) Case 2: Influence of the MOC fuel type

The MOC fuel type led to the natural circulation flow from 2.8 h to 6.0 h, as shown in Fig. 8(b). Similar to the analysis result for the EOC fuel type, in this case as well the pressurizer and surge line were cleared during the natural circulation. However, the HL nozzle experienced creep rupture after a long time.

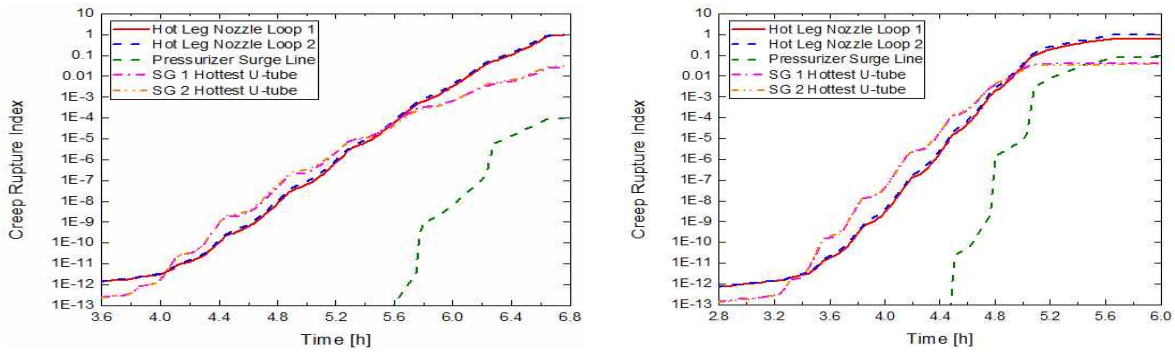

(a) Creep rupture damage index (case 1) (b) Creep rupture damage index (case 2)

Figure 8. STSBO analysis results (sensitivity cases).

4. CONCLUSION

In this paper, a best-estimate analysis was conducted to evaluate the creep rupture characteristics of the RCS pressure boundary for potential long-term and short-term SBO accident sequences of a reference PWR (APR1400), based on the MELCOR-CFD coupled analysis. Timings of the key events for the base scenarios of both accidents were summarized in Table 3. Together with this, relevant sensitivity analyses were carried out to explore the influence that particular MELCOR modelling options and plant conditions have in estimating the RCS creep rupture characteristics. The following points summarize the main results of the present analyses and relevant insights.

- The LTSBO base scenario, in which the TD-AFWP provides the feedwater to one SG for 8 h, indeed led to a creep rupture of the HL nozzle, but the SG U-tubes maintained their integrity. Even if the stress factor of the SG tubes was augmented by 1.5 times, as through sensitivity case 1, the HL nozzle ruptured prior to the creep rupture of the SG tubes. In the case that the MSSV was stuck open, as in sensitivity case 2, the SG tube ruptured first, and shortly after a subsequent HL nozzle creep rupture took place.
- The STSBO base scenario, in which all means to remove the FP decay heat inside the RCS pressure boundary are unavailable, led to a failure of the RPV LH but with no additional creep rupture of the RCS pressure boundary. In contrast, the HL creep rupture happened first in the case that the BOC and MOC fuel types were considered, as shown in the respective sensitivity cases.
- The foregoing results imply that the MSSV stuck-open failure could be a dominant contributor to the

TI-SGTR risk, at least for the APR1400 LTSBO sequence, compared to the other plant conditions.

- The present analysis results are specific to the APR1400 SBO accident, but relevant insights could be informative in understanding further progressions of severe accidents that might be induced by SBO, and also in establishing the corresponding coping strategies to similar high-pressure accident sequences.

ACKNOWLEDGEMENT

This study was carried out as part of the 'Development of the Level 2&3 PSA Technologies based on the State-of-the-Art Technology (L16S059000)' project, which was funded by the Central Research Institute (CRI) of the Korea Hydro and Nuclear Power (KHNP) Co., Ltd. This work was also partially supported by the Ministry of Science, ICT, and Future Planning of the Republic of Korea and the National Research Foundation of Korea (NRF-2020M2C9A1061638).

REFERENCES

Ahn, K.I., Hwang, S.W. (2017). "The KHNP SOARCA Project: Development Strategy," *KHNP Severe Accident and SOARCA Workshop*, Sadia National Laboratories (SNL), Albuquerque, NM, April 17.

ANS. (2014). *Decay Heat Power in Light Water Reactors*. ANSI/ANS-5.1-2014, American Nuclear Society (ANS), USA.

Bang, Y.S., Jung, G.H., Lee, B.C., Ahn, K.I. (2012). "Estimation of temperature-induced reactor coolant system and steam generator tube creep rupture probability under high-pressure severe accident conditions," *Journal of Nuclear Science and Technology*, 49:8, 857-866.

INEL. (1996). Steam Generator Tube Failures, NUREG/CR-6365. INEL-95/0383, Idaho National Laboratory (INL), Idaho Falls, ID.

KHNP. (2011). Probabilistic Safety Assessment for the SKN Units 3&4. Korea Hydro & Nuclear Power Co. (KHNP).

KHNP. (2017). Extreme Events Coping Strategy for APR1400. A16IP39-29.2, Rev. 0, Korea.

KHNP. (2019). Development of State-of-the-Art Technology for Level 2&3 PSA: Final Report. KHNP-2019-50003339, Korea Hydro & Nuclear Power Co. (KHNP).

Kim, H.G. (2017). The Design Characteristics of Advanced Power Reactor 1400. IAEA-CN- 164-3S09.

RETech. (2019). Computational Fluid Dynamics Analysis for the Improvement of the KHNP-SOARCA model. Technical Report for KHNP-SOARCA, RETech Co., Ltd., Korea.

Ryman, J.C. (2000). *ORIGEN-S Data Libraries (SCALE 6 Code Manual)*. NUREG/CR-0200, Vol.3, Rev. 6, Vol. 3. M6, U.S. Nuclear Regulatory Commission (NRC), Washington, DC.

SNL. (2017). MELCOR Computer Code Manuals (Vol.1): Primer and Users' Guide, Version 2.2.9541. SAND2017-0455, Prepared for U.S. Nuclear Regulatory Commission, Sadia National Laboratories (SNL), Albuquerque, NM.

USNRC. (1998). Risk Assessment of Severe Accident-Induced Steam Generator Tube Rupture. NUREG-1570, SGTR Severe Accident Working Group, U.S. NRC, Washington, DC.

USNRC. (2004). CFD Analysis of Full-Scale Steam Generator Inlet Plenum Mixing During a PWR Severe Accident. NUREG-1788, U.S. NRC, Washington, DC.

USNRC. (2010). Computational Fluid Dynamics Analysis of Natural Circulation Flows in a Pressurized-Water Reactor Loop under Severe Accident Conditions. NUREG-1922, U.S. NRC, Washington, DC.

USNRC. (2012). State-of-the-Art Reactor Consequence Analyses Report. NUREG-1935, U.S. NRC, Washington, DC.

USNRC. (2013). State-of-the-Art Reactor Consequence Analyses Project, Volume 2: Surry Integrated Analysis. NUREG/CR-7110, Vol. 2, Rev.1, U.S. NRC, Washington, DC.

USNRC. (2016). Consequential SGTR Analysis for Westinghouse and Combustion Engineering Plants with Thermally Treated Alloy 600 and 690 Steam Generator Tubes. NUREG-2195 (Draft), U.S. NRC, Washington, DC.